RSC Advances

ROYAL SOCIETY OF CHEMISTRY

www.rsc.org/advances

Osteoblast compatibility of minerals substituted hydroxyapatite reinforced Poly (Sorbitol Sebacate Adipate) nanocomposites for bone tissue application†

Govindaraj Dharman[a], Rajan Mariappan[a,*], Murugan A. Munusamy[b], Bala Kumaran, M[c], and P.T. Kalaichelvan[c]

*[a]*Department Of Natural Products Chemistry, School of Chemistry, Madurai Kamaraj University, Madurai 625021, India.*Phone: +91 9488014084. E-mail Id: rajanm153@gmail.com*

[b]*Department of Botany and Microbiology, College of Science, King Saud University, Riyadh, Kingdom of Saudi Arabia.*

[c]*Centre for Advanced Studies in Botany, School of Life Sciences, University of Madras, Guindy campus, Chennai – 600 025, India.*

Abstract

The main focus of this investigation is to explore minerals (M) substituted hydroxyapatite (M-HAP) as reinforcing agents to strengthen Poly (Sorbitol sebacate adipate) (PSSA), a biodegradable polymer for soft and hard tissue applications while not considerably compromising their biocompatibility. PSSA strengthened with different weight percentage of M-HAP nanocomposite was synthesized using a microwave irradiation technique. The functional groups within the nanocomposites were determined by Fourier transform infrared (FT-IR) spectroscopic and X-ray diffraction (XRD) analysis. X-ray photoelectron spectroscopy (XPS) further showed the interface interaction between the M-HAP and PSSA. The morphological and elemental analysis was obtained from field emission-scanning microscopy (FE-SEM) equipped with energy-dispersive X-ray (EDX) spectroscopic analysis and transmission electron

microscopy (TEM). The addition of M-HAP greatly increased the mechanical, thermal properties and improved the protein adsorption ability. *In vitro* bioactivity in simulated body fluid (SBF) experiment and human osteosarcoma MG63 (HOS MG63) cells proliferated on the M-HAP/PSSA shows that the nanocomposite has sensible cell biocompatibility. All these observations suggest that the M-HAP/PSSA nanocomposites will be promising biomaterials for bone tissue engineering applications.

1. Introduction

The most vital research part in biomedicine is that the improvement of nanocomposite biomaterials for appropriate hard and soft tissue replacement implants.[1] Huge efforts have been invested in the development of synthetic nanocomposites materials that mimic the physical and chemical properties of natural bone and tissues.[2] Living systems are composed of networks of interfacing biopolymers, ions and metabolites.[3] Such a ions particles like hydroxyapatite [$Ca_{10}(PO_4)_6(OH)_2$], HAP], it has involved a great deal of attention in biomedical applications as a result of its close likeness in chemical composition with the mineral a part of natural bone and teeth.[4] However, these materials are not mechanically well-matched with bone due to their poor mechanical properties, such as low impact resistance and brittle nature, which does not permit for their use in load-bearing orthopedic applications.[5] Natural bone is also contained trace amount of ions like Mn^{2+}, Mg^{2+}, Sr^{2+} and Zn^{2+} and anions like PO_4^{3-}, CO_3^{2-}, which influence the physical properties.[6-7] From this evidence, HAP can be capable of accepting ions within its lattice. Consequently, the ionic inclusion such as magnesium (Mg), strontium (Sr) and zinc (Zn) into HAP bio-ceramics has been of huge attention for the biological process after implantation. Magnesium plays an important role in preventing osteoporosis in human bone.[8]

Strontium is a bone-seeking element that exhibits the beneficial effect on bone growth.[9] Zinc also has the stimulatory effect on bone formation *in vivo*.[10]

In this way Sr^{2+}, Mg^{2+} and Zn^{2+} as vital elements, were found to be very effective in enhancing the structural stability and biological properties apatite. Both *in-vivo* and *in-vitro* studies have clearly indicated that Sr^{2+}, Mg^{2+} and Zn^{2+} influence the mineral metabolism during the osseous tissue remodelling process and enhance pre osteoblastic cell multiplication.[11] Since there is not yet a single material that fulfils all the necessary requirements for biomedical applications, nanocomposites have been developed. Therefore, there is a growing curiosity in nanocomposite materials.[12]

Moreover, such bioactive nanocomposite materials should spontaneously bond to and put together with bone in the living body.[13]Recently, much attention has been focused on hydroxyapatite/polymer nanocomposites. Ceramic/polymer nanocomposites may be synthesized to possess hardness, bending, compressive, and tensile strengths that are higher than conventional ceramic composites but are more similar to physiological bone.[14]In the ceramic/polymer nanocomposite, especially those containing biodegradable polymers such as poly (glycolic acid),[15] Poly (2-hydroxyethyl methacrylate)[16] poly (D, L-lactic-co-glycolic acid),[17-18] poly (Sorbitol sebacate) (PGS),[19]chitosan– poly ethylene glycol,[20]chitosan-PEG-gelatin,[21]chitosan/poly lactic acid/poly ethylene glycol/gelatin,[22] have the efficiency of divalent ions binding properties and extremely interesting applications in the biomedical field. Along with these biodegradable polymers, poly (sorbitol sebacate adipate) (PSSA) is a novel, one of the most important polymer group used in biomaterials research.[23-25] It is a type of biodegradable polymer with good biocompatibility.[23, 26-27]Recently, many researchers have introduced large quantity of HAP reinforced polymers composites.[28-30] This is due to their poor mechanical

properties of unsubstituted hydroxyapatite.[5] In the present work, PSSA elastomers are reinforced with small quantities of (10 Wt. %) M-HAP to achieve better the mechanical, thermal and biological properties.

To the best of our knowledge, there are no reports on the combination of M-HAP with PSSA nanocomposites by microwave method. An innovated synthesis method for the fabrication of M-HAP/PSSA nanocomposites via microwave pre polymerization which happens in a few minutes rather than days.[19, 31]In this paper, we carried out mimicked the size scale of minerals substituted hydroxyapatite in natural bone and aim to fabricate novel and improved nanocomposites scaffolds. The pore nano-beads structure, mechanical, thermal, antibacterial, protein adsorption properties and cells proliferation ability were scientifically investigated. The results suggest that the newly developed M-HAP/PSSA nanocomposite scaffolds may serve as an excellent substrate for cell attachment and migration in bone tissue engineering.

2. Materials and methods

2.1. Materials

Commercially available calcium chloride tetrahydrate ($CaCl_2.4H_2O$), strontium chloride hexahydrate ($SrCl_2.6H_2O$), magnesium chloride hexahydrate ($MgCl_2.6H_2O$), zinc chloride ($ZnCl_2$), dipotassium hydrogen phosphate (K_2HPO_4), sorbitol, sebacic acid and adipic acid purchased from Aldrich Chemicals (Aldrich, India) were used for the fabrication of M-HAP/PSSA nanocomposites by microwave method. All chemicals were analytical grade and ultrapure water was used as all through the experiment.

2.2. Preparation of nano M-HAP

At first, 0.5 wt. % of the glutamic acid and 0.05 M of $CaCl_2.4H_2O$, 1wt. % $SrCl_2.6H_2O$, 1 wt. % $MgCl_2.6H_2O$ and 0.25 wt. % $ZnCl_2$ were taken in a glass beaker and stirred with vigorously a

magnetic stirrer for 30 minutes to make sure the mutual interaction and the self-assembly process was completed. The solution was adjusted to pH 9.5 using NH_4OH. At that point 0.03M, (K_2HPO_4) was added dropwise to the mixture under stirred conditioned 6h and formed a white precipitate. The mixture was placed in a microwave oven and irradiated for 120 seconds at 740W. Then, the resultant powder was thermally treated at 900°C for 2 h in a muffle furnace to obtain nano minerals substituted bioceramic.

2.3. Synthesis of M-HAP/PSSA nanocomposites

The nanocomposites preparation performed in two stages: The pre polymerization stage was performed using a microwave oven ((A CEM Discover microwave synthesizer (Model No: 908010) operating at 180/264 V and 50/60 Hz with microwave power maximum level of 300 W and microwave frequency of 2455 MHz)). The different amount of M-HAP (1 wt. %, 5 wt. % and 10 wt. %), 2 mol sorbitol, 1 mol sebacic acid was at first included into a 100 ml round-bottom flask. The mixture was subjected to microwave irradiated applied for 10 minutes with 10-second intervals at 100 W and then 0.9 mol of adipic acid was added. Followed irradiated applied for 10 minutes at 100 W is to create a prepolymer. No catalyst or any other reactant was used in this stage. Subsequently, the gel-like slurry of per polymer nanocomposite was kept in vacuum oven, the curing (post polymerization) reaction was performed at 120ºC and 1KPa in the vacuum oven for 1 hour, without vacuum for a period of time to acquire M-HAP/PSSA nanocomposites with various degrees of cross-linking,[32]After the desired polymerization time, cooled it to room temperature solidified nanocomposite were collected and characterized. The overall time required to get ready an elastomer, as described in here, was about 3 h, which is very short when compared to the characteristic times of conventional processes that are about 2 or 3 days.[33]The pure PSSA polymer were also prepared by the same process yet without M-HAP

sources. (Optimization study for the synthesis of Poly (Sorbitol Sebacate Adipate) nanocomposites given in supplementary material section).

3. Characterization

3.1. FTIR Spectra

The distinguishing proof of functional groups in 10 wt.% M-HAP within PSSA elastomer (M-HAP/PSSA) prepolymer nanocomposite and postpolymer (curing) nanocomposite was analyzed by Nicolet 380 Fourier transform infrared (FT-IR) absorption spectroscopy (Perkin Elmer, USA)) within the scanning range of 4000 to 500 cm^{-1} using a KBr pellet technique.

3.2.XPS characterization

X-ray beam photoelectron spectroscopy (XPS) was used to quantify the elemental composition of the M-HAP and M-HAP/PSSA nanocomposite. The XPS spectra were recorded using an SSX-100 spectrometer with monochromatized X-beam Al Kα radiation (1486.6 eV). The resolution was measured as full width at half maximum of 1.0 (core-level spectrum) to 1.5 eV.

3.3. XRD Spectra

A Bruker D8 advanced XRD instrument was working for the phase identification and the crystallinity of the M-HAP/PSSA nanocomposite. Designed for the XRD experiments, Cu Kα incident radiation, a tube voltage of 40 kV and a current of 30 mA was used and the scanning angle is ranged from 10 to 80°, with a scan rate (2θ) of 0.02°.

3.4. TEM observation

The microstructure of M-HAP/PSSA nanocomposite scaffold was examined with the transmission electron microscope (TEM-JEOL JEM 2100 Co., Tokyo, Japan) with a 200 kW. The samples for TEM analysis was prepared by M-HAP/PSSA nanocomposite dispersing in ethanol, followed by sonication step for 10 min. Then, a drop of the suspension was deposited on

copper coated carbon grid with 200 meshes and the solvent was allowed to evaporate.

3.5. Field emission scanning electron microscopy

The morphological characteristics and chemical composition of the M-HAP/PSSA nanocomposite were examined FE-SEM (Curl Jdiss Supra 40-2007, Germany) operated at an accelerating voltage of 10 kV equipped with EDAX. The samples for FESEM were prepared by placing the nanocomposites on the conductive carbon tape.

3.6. Mechanical characterization

Tensile tests were performed the CMT4104 testing machine (Shenzhen SANS Testing Machine Co. Ltd., China) furnished with a 50 N burden cell at 31°C. In brief, the nanocomposite specimen (25mm length x 2mm width x 1 mm thickness) was tried at a rate of 50 mm/min to break. The stress–strain bend and Young's modulus were achieved. Samples (4–6) were measured and their values were averaged.

3.7. Differential scanning calorimeter

Differential scanning calorimeter (DSC 822e, Mettler Toledo) was applied to investigate the thermal property of the synthesized nanocomposites in a nitrogen atmosphere with the flow rate of 200 ml/min.

3.8. *In vitro* soaking test

The investigation of *invitro* bioactivity of nanocomposites was done by absorbing 50 ml SBF with pH was 7.4 at the temperature of 37± 1°C. The ion composition of simulated body fluid is almost equal to ionic concentrations of human blood plasma and it was prepared according to the literature Kokubo.[34] Cleaned samples of size 2 × 2 cm were immersed and stored in the incubation apparatus for 1, 3 and 7 days at the temperature of 37°C. The microstructure of surface was tested before and after soaking in SBF by FE-SEM.

3.9. Antibacterial properties

The *in-vitro* antibacterial properties of the pure HAP, M-HAP, PSSA and 10 Wt% of M-HAP/PSSA nanocomposite using the bacterial strain of Escherichia coli (ATCC#25922) by the agar disc diffusion technique. The microorganisms were prepared from fresh overnight broth cultures (Tripton soy broth with 0.6% yeast extract–Torlak, Serbia) that were incubated at 37^{o}C. The agar disc diffusion test was performed at Muller-Hinton agar. The diffusion technique was carried out by pouring agar into Petri dishes to form 4 mm thick layers and adding dense inoculums of the tested microorganisms in order to obtain semi confluent growth. Petri plates were left for 10 min to dry in the air and after that, discs were prepared from Whatmann filter paper and immersed in 50 and 100µL concentration of as synthesized nanocomposites and then the discs were placed at equal distance and incubated for 24 h at 37^{o}C. The antibacterial activity was measured as the zone of inhibition (mm) around the disc.

4. Protein adsorption

Protein adsorption was performed by incubating the nanocomposite in PBS (phosphate buffered saline, 0.1m, pH=7.4) containing 5% FBS (fetal bovine serum). The disk-like specimens with the size of 15.5–16.5 mm in width and 370.1 mm in thickness were used. Before incubation in the medium includes proteins, the specimens were pre-treated with ethyl alcohol for 30 min and then washed with PBS three times overnight under mild shaking. Specimens were then put into 24-well culture plates (one sample for each well) and 1.5 ml FBS/PBS solution was added into each well. The nanocomposite was incubated at 37^{o}C for a select incubation period. The concentration of the protein in the FBS/PBS solution was then rated with a commercial protein assay kit, BCA (Pierce, Rockford, IL), BSA (using bovine serum albumin) standards. The amount of absorbed

proteins was decided by subtracting the amount of proteins port in the FBS/PBS solution after adsorption from the amount of proteins in control FBS/PBS solution (without sample) under the same incubation conditions.

4.1. *In vitro* cell culture experiments

HOS MG63 cells obtained from National Centre for Cell Science (NCCS), Pune, India were cultured in minimal essential media (Hi Media Laboratories) supplemented with 10% Fetal Bovine Serum (FBS), Streptomycin (100 U/ml) and Penicillin (100 U/ml) (Cistron laboratories). The cell culture was then incubated under the humidified atmosphere (CO2) at 37 °C. The samples under examinations were sterilised in the autoclave at 120 °C during 2 h and placed in 96 well cell culture plates.

Assessment of cell broadening was achieved used the MTT (3–4,5-dimethylthiazol-2yl{-2,5-diphenyl-2h-tetrazoliumbromide) assay. The medium in the cell-loaded nanocomposite culture plate was detached after cultured for 1, 3 and 7, and 2 ml MTT solution was added to each one example. Taking after 4 h incubation at 37 °C in an air atmosphere containing 5% CO_2, and DMSO was used to dissolve the formazan crystals, and the optical densities (OD) were determined using a spectrophotometric microplate reader at 570 nm compared with DMSO blank, which is linear correlations between cell numbers. The controls (empty wells without nanocomposite) were treated in the similar manner.

5. Results and discussion

Many synthetic materials, as well as biopolymers, bioceramics, bimetallic materials and their nanocomposites are now in use for bone and tissue repairing.[35] However, none of them will perform as absolute as the physiological bone. Therefore, there is a real require for novel biomaterials for bone defect repair. As a matter of fact, minerals substituted hydroxyapatite/poly

(sorbitol sebacate adipate) nanocomposites are studied during this regard. Nevertheless, to the best of our knowledge, no report has discussed the chemical reactivity, mechanical and bioactivity such nanocomposite.

5.1. Characterization of chemical structure

FT-IR data has showed very vital information about the interactions between M-HAP and PSSA matrix. Figure 1a-c, revealed the FT-IR spectra of M-HAP, prepolymer and postpolymer of M-HAP/PSSA nanocomposite (10 wt% M-HAP). The peaks at 1,092 cm^{-1} and 1,032 cm^{-1} were assigned to the vibration of a phosphate group of M-HAP structure. The peaks at 1,630 and 3,455 cm^{-1} were corresponded to the hydroxyl group in the adsorbed water, the stretching modes of the OH^- ions appear at 3572 and 602 cm^{-1}, respectively in Figure 1a.[6] The stretching vibration peak of OH^- in carboxyl groups (–COOH) of PSSA at 3382 cm^{-1} (broad peak in Figure 1b) vanished. Meanwhile a new weak $–COO^-$ peak was appeared at 1410 cm^{-1} in the nanocomposite spectrum (Figure 1c). It can be implicit that carboxyl groups (–COOH) of PSSA were ionized to form $–COO^-$ ions during the nanocomposite formation. Then, COO^- ions would bind with Ca^{2+} ions of M-HAP and a new weak carboxyl-calcium carboxyl linkage might be formed (Figure 1c).[36] Meanwhile, the vibration peaks at 2932 and 2857 cm^{-1} of methyl groups in the PSSA spectrum (Figure 1b) decrease to 2931, and 2855 cm^{-1} in the nanocomposite[36] (Figure 1c), respectively. These results signify some molecular interactions between the M-HAP and PSSA in the nanocomposite. While phosphate peaks of M-HAP and many peaks of PSSA from 550 to 1150 cm^{-1} co-occur in the spectrum of nanocomposite, it can be observed that PO_4^{3-} peaks of M-HAP at 1032 and 1092 cm^{-1} shifted back to 1027 and 1086 cm^{-1} in the nanocomposite. This result also implied some molecular interactions between the PO_4^{3-} in M-HAP and the PSSA in the nanocomposite.[37]

5.2. XPS analysis

Figure 2 is the XPS curve of M-HAP (a) and the M-HAP/PSSA nanocomposite (b). The binding energy of calcium (Ca), strontium (Sr), magnesium (Mg), zinc (Zn), phosphor (P), oxygen (O) has some difference between M-HAP (O: 531.5, Ca: 351.8 & 347.3, Mg: 49.8 Zn: 1022.5 Sr: 134.5 and P: 134.5 eV) and in the nanocomposite (O: 531.6, Ca: 351.9 & 347.4, Mg: 49.9 Zn: 1022.6 Sr: 134.6 and P: 134.6 eV).[38-40] Comparison of the binding energy of Ca, Mg, Sr, Zn, O and P in M-HAP with that in the nanocomposite shows that the binding energy of Ca, Mg, Sr, Zn, O and P increases in the nanocomposite, this means that there are some interface interaction or bonding present between the M-HAP and PSSA.

5.3. X-ray Diffraction (XRD)

The XRD patterns of the M-HAP/PSSA nanocomposites are exhibited in Figure S1. The XRD pattern of PSSA reveals its semi-crystalline character. The XRD patterns of the nanocomposites (M-HAP/PSSA) display additional peaks at 2θ = 25° (low intensity), 32° and 35° which correspond to M-HAP peaks.[6] The peaks at 32 and 35° tend to increase in intensity with the increase in the M-HAP concentration. The XRD study confirms the vicinity of M-HAP inside the PSSA polymer matrix.

For the XRD patterns of M-HAP/PSSA nanocomposite soaked in SBF for different days 1, 3, and 7 days. The peaks (Figure. S 2 (b-c)) become sharper and intense, which is a clear designation that the crystalline. Thus, as the soaking time is increased, the CaP crystals depositions on nanocomposite exhibited increased crystalline.[41,42]Hence, from this XRD pattern it could be concluded that, the soaking time plays an important part in the mastery of phase of the CaP depositions on nanocomposite with desired crystallinity, which might be suitable for tissue biocompatibility.[41]It clearly discussed blow (Figure. 7).

5.4. TEM micrographs

In order to confirm the presence of M-HAP in the M-HAP/PSSA nanocomposite, TEM analysis was performed and the micrograph is shown in Figure 3. It shows that rod like M-HAP crystals are still in the range of nanometer level and receive a good dispersive property in the polymers, which sustains a positive outcome on the mechanical, thermal and biological properties of the M-HAP/PSSA nanocomposite scaffold.[43]

5.5. Morphology observation

The FESEM micrographs in Figure 4 reveal the microstructure of the prepolymer and different weight percentage of M-HAP in PSSA nanocomposite. The addition of M-HAP significantly altered the surface morphology of the polymer matrix.[44] The surface of the prepolymer in Figure 4a appeared as smooth (gel) and almost fully dense. On the other hand, when nanocomposite was cured, it became rougher and microporous beads, as shown in Figure 4b. The pore size was ranged from a few to several hundred nanometers. When the amount of M-HAP is less than 5 wt. %, most of these porous beads were not isolated from each other. However, when the M-HAP content was increased from > 5 wt. %, the beads were become larger in size and interconnected (Figur 4 c-h). These changes in the microstructure of the nanocomposite were attributed to the gradual weakening of the intermolecular interactions such as the M-HAP bonding within the PSSA network, caused by the increased M-HAP content. The elemental composition of M-HAP (10 Wt. %) in PSSA investigated by EDX analysis (Figure 4 i). The intense peak of Ca, Sr, Mg, Zn, P, and O confirms the formation of nanocomposite (M-HAP/PSSA).[6] Therefore, this nanocomposite is the consideration to be good structures for cell proliferation due to the presence of minerals in HAP. The porous bead structure of the M-HAP/PSSA nanocomposite scaffold would be expected to increase the number of cells adhering to the membranes on implantation

and enhance the membrane-tissue attachment by allowing the tissue to infiltrate. In addition, the interconnecting porous beads network in nanocomposite may be advantageous to the circulation of body fluid and blood.[45]

There were clear minerals substituted hydroxyapatite-polymer interface, which confirmed the conclusions which were drawn from the FTIR and XPS observations that there was good miscibility between the two phases, M-HAP, and PSSA. In addition, the existence of a homogeneous porous beads structure in the entire M-HAP/PSSA nanocomposite indicated that the combined use of the microwave method and the dynamic curing technique in this study was very efficient to mix PSSA and M-HAP particles and made it possible to obtain a uniform nanocomposite with a high percentage of M-HAP.

5.6 Mechanical properties

The controlled integration of organic and inorganic components confers natural bone with superior mechanical properties.[46] The mechanical property of M-HAP/PSSA nanocomposite is one of the main key factors determining both their clinical operation and bone therapeutic ability.[47] As depicted in Figure 5, it can be visually perceived clearly that with incorporating M-HAP content from 1wt% to 10 wt% in the nanocomposite, the tensile strength and the modulus of nanocomposites significantly increased, meanwhile, the elongation at break of the nanocomposites were reduced remotely. The results are presented in table S2, compared with the pure PSSA elastomer, the nanocomposite shows a lower tensile strength and strain at the failure; conversely a higher initial slope in their stress–strain curves. On the other hand, as the M-HAP content was increased, the elastic modulus of the nanocomposite exhibited a primary rapid increase followed by a gradual decrease. PSSA stretched macromolecule chains were formed during stretching between the M-HAP particles, induced by the slippage of macromolecule

chains on the M-HAP particle surface, most important to improved strength and hardiness.[48] This occurrence was cognate to the mechanism of PSSA elastomer reinforced high tensile strength is the resolution of the interface interaction, which mainly refers to the chemical absorption of polymer chains to the M-HAP nanoparticles surface.

Mechanical tests show that the tensile strength of the M-HAP (10Wt. %) in PSSA nanocomposite is approximately 22.10 MPa, whereas that of pure PSSA is almost 16.10 MPa. Therefore, the results are higher with minerals substituted hydroxyapatite being incorporated into the PSSA nanocomposite, possibly due to the high mechanical strength of M-HAP.[6] Highest M-HAP (10Wt. %) content in PSSA nanocomposite is higher than the standard 15 MPa for surgery-HAP application according to ISO 13779-2.[49]

5.7. Thermal analysis of M-HAP/PSSA nanocomposite

As per the results of DSC curves of nanocomposite are shown in Figure 6 and data listed in table S2. The M-HAP/PSSA scaffold showed an obvious glass transition temperature, around 39.92 to 42.70 °C. The glass transition temperature (Tg's) was observed to rising loading concentration, attains a minimum of 40.91°C at 1 wt. % of M-HAP. However, the M-HAP % of weight was increased from 1 to 10 wt. %, Tg's was increased to 42.51°C. Because the Tg's is extremely dependent on polymer cross-linkage, hydrogen bonding, physical interactions between M-HAP particles and PSSA polymer matrix.[50] We noticed that the Tg's of the nanocomposites shifted to higher temperatures while increasing the loading of M-HAP. Usually, nanoceramic increases the Tg's of nanocomposite materials through nanofiller polymer interaction, especially when the interaction is strong enough to block the segmental motion.[51] Hence, the values of Tg's pointed out that the M-HAP/PSSA nanocomposites are solid at room temperature.

5.8. SBF immersion test

The necessary requirement for synthetic material to bond with living bone is the formation of bone-like apatite on its surface when bio-composites in the immersion in simulated body fluid.[52] This means that *invitro* bone bioactivity of a material can be predicted from the apatite development on its surface in SBF.[52] Figure 7 displays the formation of apatite on the surface of 10wt. % M-HAP nanocomposite during the test periods. The *invitro* testing proved the bioactive properties of the M-HAP/PSSA nanocomposite. A very small amount of CaP crystals was formed on M-HAP/PSSA after soaking in SBF for 1 day (Figure 7a). As the immersion day's increases, they continued to grow and steadily filled the needle and finally, covered over the entire surface of M-HA/PSSA nanocomposite.[53] Following 3 days soaking nanocomposite in SBF the accompanying perception was noticed in Figure 7b, the surface of M-HAP/PSSA nanocomposite CaP needles were irregularly covered by a layer of apatite. The deposition of almost fully covered bone needle-like apatite was observed on nanocomposite after 7 days of soaking in SBF (Figure 7c). The high magnification FE-SEM micrograph [the inset of figure 7 (a-c)] shows that the CaP nano-needles particles were composed of numerous crystals on nanocomposite with the size ~100 nm in diameter. It can also be expected that the same will occur under *in vivo* conditions; that is, a new apatite-like phase should form on the surface of the CaP crystals after their implantation, either as a pure ceramic or as a composite.[41]These results mean that the M-HAP nanoparticles content included PSSA somewhat affected the formation of bone needle-like apatite.

5.9. Antibacterial activity

The antibacterial activity of M-HAP/PSSA was analyzed and compared with the pure HAP, M-HAP and pure PSSA (Figure S 3). There was no important change in the activity found in pure

PSSA and pure HAP.[54]This is clear that PSSA does not influence the antibacterial property of M-HAP. The zone got for M-HAP was found to be ~10–12mm at 100µL concentration of the synthesized nanomaterials, where with respect to the 10 Wt% of M-HAP in PSSA, the restraint zone was discovered to be around ~9–12mm which demonstrated the presence of antibacterial property of the as-synthesized nanomaterials samples.

6. Protein adsorption

M-HAP/PSSA composite scaffolds with different amounts of M-HAP were incubated in FBS/PBS solution to investigate protein adsorption. For all M-HAP/PSSA composite scaffolds, the protein adsorption reached equilibrium in 30 h and there was no significant increase in protein adsorption during further incubation (Figure. S4 A). The incorporation of M-HAP increased the protein adsorption increased (M-HAP (5Wt. %) /PSSA and M-HAP (10Wt. %) /PSSA composite scaffolds absorbed[55] (Figure. S4 B). The Scaffolds with nano-beads texture absorbed about four times greater amount of protein than those with the smooth surface. These results suggested that the protein adsorption on the scaffolds could be regulated by the content of M-HAP and its pore beads morphology of the nanocomposite.

6.1. Cell viability proliferation

The cell proliferation on the nanocomposite was assessing using MTT test.[56-57] Figure 8 demonstrates the morphology and optical density (OD) estimation of the cells attachment on the nanocomposite for different days of incubation. Allowing to the data, it can be observed that MG63 increased with time during the *in vitro* culture period, and the M-HAP/PSSA nanocomposite group has an evident proliferation tendency, implying the nanocomposite did not restrict the cell multiplication,[23-27] which demonstrates the nanocomposite is non-toxic. At 3 days, MG63 live cells on the surface of the nanocomposite and increase well compare than the

first day (Figure 8 b,c). After 7 days culture, more and more cells attached tightly with their filopodium and lamellipodium, and elongated to every corner of scaffold[58] (Figure 8 d). Based on these results, we took it for granted that the novel M-HAP/PSSA composite nanocomposite had good cell biocompatibility *in vitro*.

7. Conclusion

The establishment of synthetic biodegradable nanocomposite those mimic the natural elastic properties is a main goal for hard and soft tissue fabricating. The incorporation of ceramic nanoparticles (M-HAP) in PSSA has promoted the mechanical, thermal, protein adsorption and biological properties of orthopedic materials as compared to PSSA. Case in point, M-HAP (10Wt.%)/PSSA nanocomposites demonstrated a greater tensile strength than the PSSA. The glass transition temperature of the M-HAP (10Wt.%)/PSSA nanocomposites were superior due to the confinement of the mobility of the polymer segments caused by the addition of M-HAP. The M-HAP is demonstrated a good compatibility with adipic, as a result, M-HAP particles were finely dispersed in a polymer matrix. Coupled with prior studies indicating greater osteoblast functions the mixture of PSSA with nanoceramics may provide better candidate materials for more prominent biomaterials applications. Hence it is clearly evident that the combination of the M-HAP/PSSA with a physically powerful, biocompatible, be nontoxic, and well-detached nanoceramic part can be extremely capable of customizing all properties of our next generation orthopedic/dental biomaterials.

Acknowledgements

One of the authors, M. Rajan, is grateful to the University Grant Commission (UGC), Government of India, for providing financial assistance under the scheme of “UGC-BSR Research Start-Up Grants” (Ref: No.F.30-21/20014 (BSR). M. Rajan thanks the PURSE

program for the purchase of SEM& FTIR and the University Grants Commission, New Delhi, for funds under UPE programs for the purchase of a high resolution transmission electron microscopy (HRTEM).

We are grateful to the Director, CAS in Botany, School of Life Sciences, University of Madras for providing adequate laboratory facilities to perform the cell lines studies.

The authors would like to extend their sincere appreciation to the Deanship of Scientific Research at King Saud University for its funding of this research through the Research Group project No-RGP-1435-057.

References

1. C. Sanchez, B. Julian, P. Belleville, M. Popall, J. Mater. Chem., (2005), 15, 3559–3592.

2. L.E. Freed, G.C. Engelmayr, J.T. Borenstein, F.T. Moutos, and F. Guilak, Adv Mater., (2009), 21, 3410–3418.

3. J. A. Prescher, and C. R. Bertozzi, Nature Chemical Biology (2005), 1, 13 - 21.

4. G.Z. Hui, Z. Qingshan, and W. Yong, Chem. Mater, (2005), 17, 5824-5830.

5. J.H.G. Rochaa, A.F Lemosa, S. Agathopoulosa, P.Valériob, S. Kannana, F.N. Oktara, and J.M.F. Ferreira, Bone, (2005), 37, 850–857.

6. S. C.Cox, P. Jamshidi, L. M.Grover, and K.K. Mallick, Materials Science and Engineering , (2014), 35, 106–114.

7. S. J. Kalita, and H. A. Bhatt, Materials Science and Engineering: C, (2007) 27, 837–848.

8. R. K. Rude, Journal of Bone, Mineral Research, 1998, 13, 749-758,

9. S. P. Nielsen, Bone, 2004, 35, 583-588.

10. K. Cheng, J. Zhou, W. Weng, S. Zhang, G. Shen, P. Du, Thin Solid Films, 2011, 519, 4647-4651.

11. S. Bodhak, S. Bose, A. Bandyopadhyay, Mater. Sci. Eng., C, 2011, 31, 755.

12. H. Liu, and T. J. Webster, International Journal of Nanomedicine, (2010), 5, 299–313.

13. N. M. Alves, I. B. Leonor, H. S. Azevedo, R. L. Reis, J. F. Mano, J. Mater. Chem., (2010), 20, 2911–2921.

14. C. Laurencin, Y. Khan, and S. F. El-Amin, Expert Rev Medical Devices, (2006), 3, 49-57.

15. X. Z. Zhou, V. Y.Leung, Q. RDong, K.M.Cheung, D. Chan, and W. W. Lu, Int J Artif Organs, (2008), 31, 480-489.

16. J. Song, E. Saiz, and C. R. Bertozzi, J. AM. CHEM. SOC, (2003), 125, 1236-1243.

17. D. Cheng, X. Cao, H.Gao, J. Hou, W. Li, L. Hao and Y. Wang , RSC Adv,(2015), DOI: 10.1039/C4RA15561K.

18. I. S. Magdiel, K. S. K. Pheng, H. E. Bao, X. Sijing, Z. Xinxin, K.D. Gautom, T. Timothy Thatt-Yang, S.C.L. Joachim, T. L. David, and K. W. Ng, Journal of Biomedical Materials Research Part A,(2013), 101A, 633–640.

19. Y. Li, and G. A. Thouas, RSC Adv, (2012), 2, 8229-8242.

20. M. Rajan, and V. Raj, Int J Pharm PharmSci, (2012), 4, 255-259.

21. M. Rajan, V. Raj, A. A. Al-Arfaj, and A.M. Murugan, International journal of Pharmaceutics, (2013), 2, 514-522.

22. M. Rajan, and V. Raj, Carbohydrate Polymers, (2013), 1, 951-958.

23. Yuan Li, G.A. Thouas, Q. Chen, RSC Adv., (2012), 2, 8229–8242

24. Q. Chen, S. Lianga , G. A. Thouas, Soft Matter, (2011), 7, 6484–6492.

25. J. A. Hunt, R. Chen, T. V. Veen, N. Bryan, J. Mater. Chem. B, 2014, 2, 5319–5338.

26. Y. Chandorkar, G. Madras and B. Basu, J. Mater. Chem. B, 2013, 1, 865–875.

27. A. Celli, P. Marchese, S. Sullalti, C. Berti, G. Barbiroli, S. Commereuc, V. Verney, Green Chem., (2012), 14, 182–187.

28. L. Lei, L. Li, L. Zhang, D. Chen, W. Tian, Polymer Degradation and Stability, (2009), 94, 1494–1502.

29. X. Zhang, W. Lang, H. Xu, X. Yana, Y. Guoa , RSC Adv., (2015),5, 21532-21543.

30. N. Koushki, A. A. Katbab, H. Tavassoli, A. Jahanbakhsh, M. Majidi, S. Bonakdar, RSC Adv., (2015), 5, 9089-9096.

31. J.Han, H.Y. Song, F. Saito, B. T. Lee, Materials Chemistry and Physics., (2006), 99, 235–239.

32. C. L. Nijst, J. P. Bruggeman, J. M. Karp, L. Ferreira, A. Zumbuehl, C. J. Bettinger, and R. Langer, Biomacromolecules, (2007), 8, 3067-3073.

33. H. M. Aydin, K. Salimi, Z. M. O. Rzayev, E. Pişkin, Biomater. Sci., 2013, 1, 503.

34. T. Kokubo, H.Takadama, Biomaterials, (2007), 27, 2907-2915.

35. S. M., Oliveira, R.L. Reis, and J. F. Mano, ACS Biomater. Sci. Eng. (2015), 1, 2−6

36. X. Yumei, L. Dongxiao, F. Hongsong, L. Xudong, G. Zhongwei, and Z. Xingdong, Materials Letters.,(2007), 61, 59–62.

37. B. Sarker, J. Hum, S. N. Nazhat, and A. R. Boccaccini, Adv.Healthcare Mater, (2014), 4,169–319.

38. A. Balamurugan, G. Balossier, P. Torres, J. Michel, and J. M. F. Ferreira, Materials Science and Engineering: C,(2009), 29, 1006–1009.

39. M. Bornapoura, N. Muja, D. Shum-Tim, M. Cerruti, and M. Pekguleryuz, ActaBiomaterialia (2013), 9,5319–5330.

40. M.Yukiko, S. Ken, Y. Tomohiko, H. Masahiro, and O. Tsuneo, Separation and Purification Technology, (2013),103,161–166.

41. L. Zhou, G. Tan, Y. Tan, H. Wang, J. Liao, C. Ning, RSC Adv., 2014, 4, 21997–22008.

42. Bora Mavis, T. T. Demirtas, M. Gumusderelioglu,G. Gunduz, U. Colak, Acta Biomaterialia ., (2009), 5, 3098–3111.

43. S. Teng, E. Lee, B. Yoon, D. Shin, H. Kim, J. Oh, Wiley InterScience., (2007), DOI: 10.1002/jbm.a.31897.

44. F. Chicatun, C. E. Pedraza, C. E. Ghezzi, B. Marelli, M. T. Kaartinen, M. D. McKee, and S. N. Nazha, Biomacromolecules, (2011), 12, 2946–2956.

45. S. J. Kalita, S. Bose, H. L. Hosick, and A. Bandyopadhyay, Materials Science and Engineering C, (2003), 23, 611 – 620.

46. J. Song, M., Viengkham, C.R. Bertozzi, J. AM. CHEM. SOC, (2005), 127, 3366-3372.

47. H. Peng, N. Poovaiah, M. Forrester, E. Cochran, Q. Wang, ACS Biomater. Sci. Eng, (2014), 1, 37–42.

48. S.H. Teng, E. J. Lee, B.H. Yoon, D.S. Shin, H.E. Kim, and J.S. Oh, J Biomed Mater Res, (2009), 88, 569-80.

49. ISO, Implants for surgery-hydroxyapatite—Part 2: Coating of hydroxyapatite, second ed., ISO 13779-2, 2008.

50. J. Jancar, J.F. Douglas, F.W. Starr, S.K. Kumar, P. Cassagnau, A.J. Lesser, S.S. Sternstein, M.J. Buehler, Polymer., (2010), 51, 3321-3343.

51. D. Weifu, R. Jingjiao, S. Dongjian, M. Piming, L. Xiao, D. Fang, N. Zhongbin, and C. Mingqing, Polymer Degradation and Stability, (2013), 98, 1790-1795.

52. Q. Wu, C. Liu, L. Fan, J. Shi, H. Jia, Q. Qi, L. Sunc and F. Chend, RSC Adv, (2013), 3,7486-7494.

53. F. Mohandes, M. Salavati-Niasari, RSC Adv., (2014), 4, 25993-26001.

54. X. Bai, K. More,C. M. Rouleau, and A. Rabiei, ActaBiomaterialia, (2010), 6, 2264–2273.

55. W. Lee, C. Loo, A. V. Zavgorodniy, M. Ghadiria , R. Rohanizadeh, RSC Adv., (2013),3, 4040-4051.

56. S.Hofmann, H. Hagenmüller, A. M. Koch, R. Müller, G. Vunjak-Novakovic, D.L. Kaplan, H. P. Merkle, and L. Meine, Biomaterials, (2007), 28, 1152–1162.

57. B. C. Heng, G. K. Das, X. Zhao, L. Ma, T. Thatt-Yang Tan, K. W. Ng, and J. Say-Chye Loo, Biointerphases, (2010), 3, 88-97.

58. K. Das, S. Bose, and A. Bandyopadhyay, ActaBiomater,(2007), 3, 573-585.

Figures

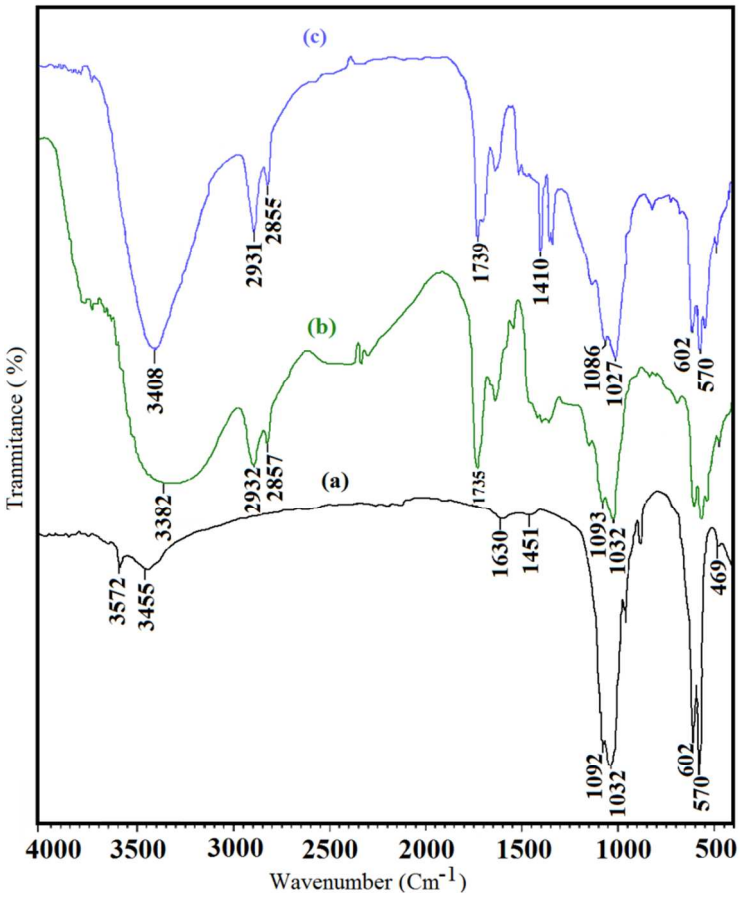

Fig. 1 IR spectra of a) Pure M-HAP, b) 10 Wt. % of M-HAP in PSSA prepolymer, c) 10 Wt. % of M-HAP in PSSA postpolymer.

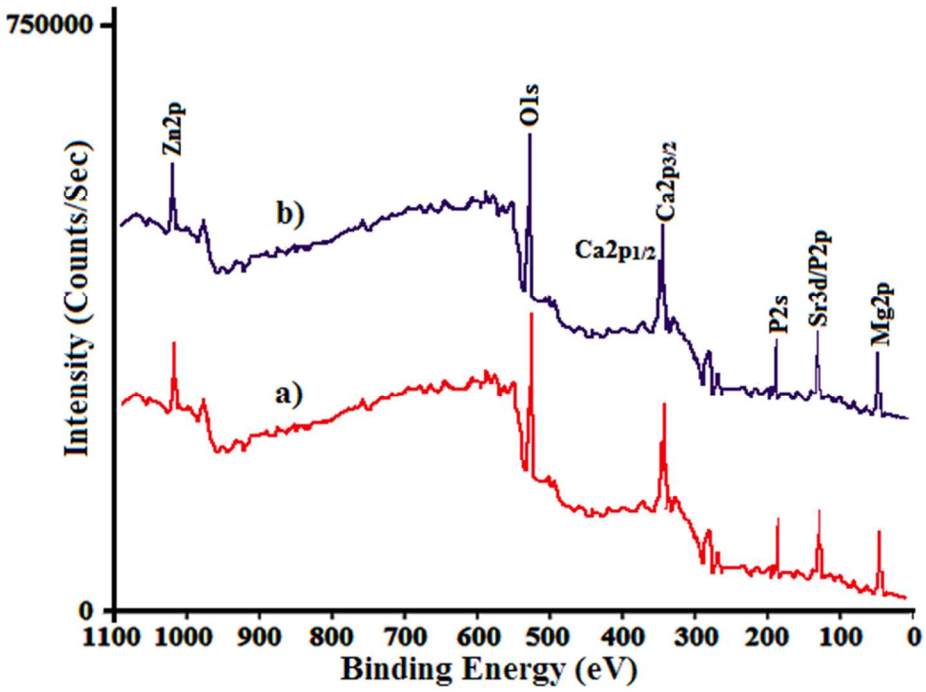

Fig. 2 XPS spectra of (a) Pure M-HAP and (b) 10 Wt. % of M-HAP in PSSA nanocomposite.

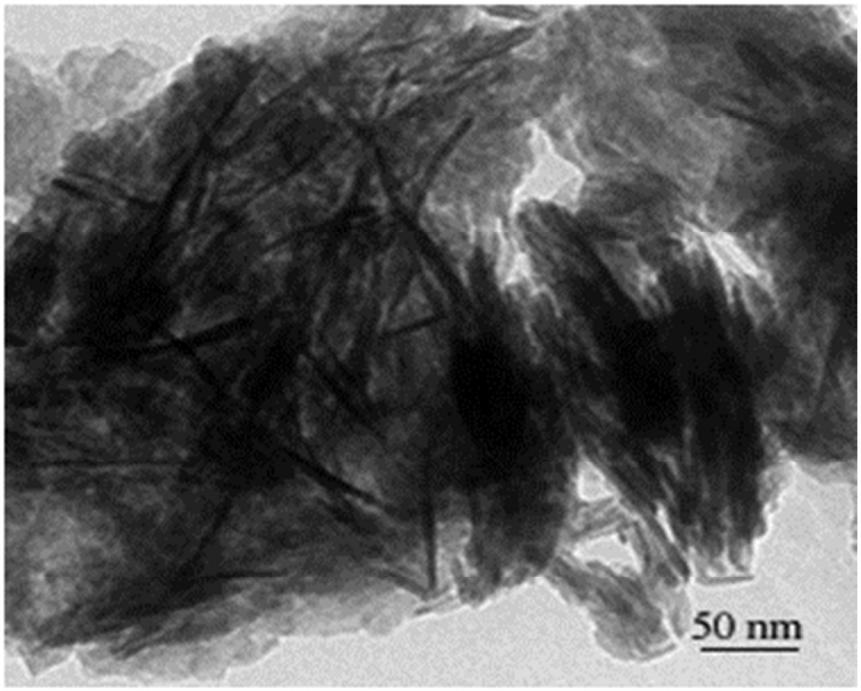

Fig. 3 The TEM photograph of 10 Wt. % of PSSA/M-HAP nanocomposite

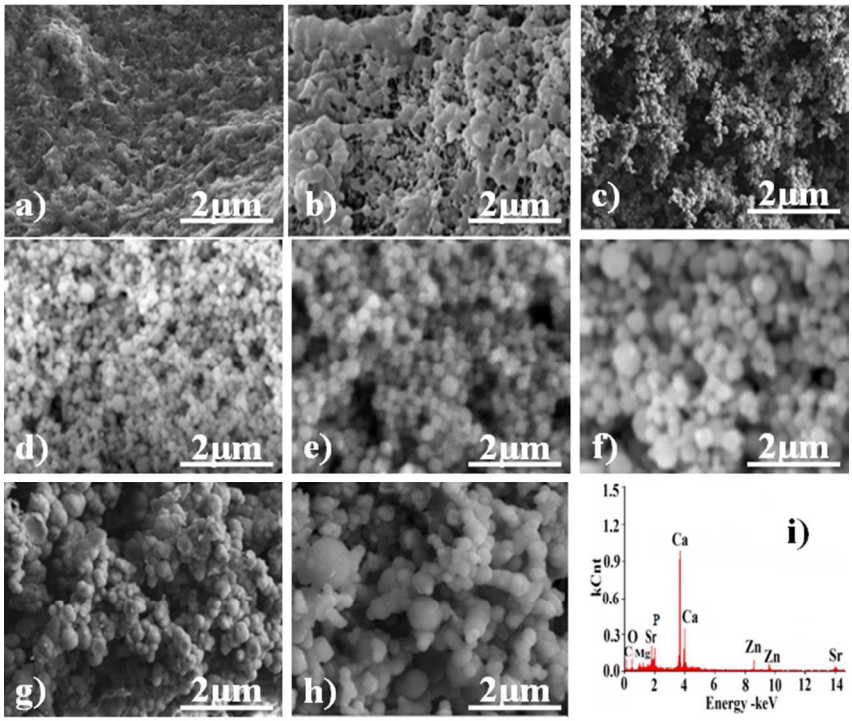

Fig.4 FESEM micrographs of surfaces of (a) Pre polymer; different weight percentages of M-HAP in PSSA postpolymers (b) 1Wt.% (c) 5Wt.% (d) 10Wt.% (d) 6Wt.% (e) 7Wt.% (f) 8Wt.% (g) 9Wt.% and (i) elemental composition of M-HAP (10 Wt.%) in PSSA.

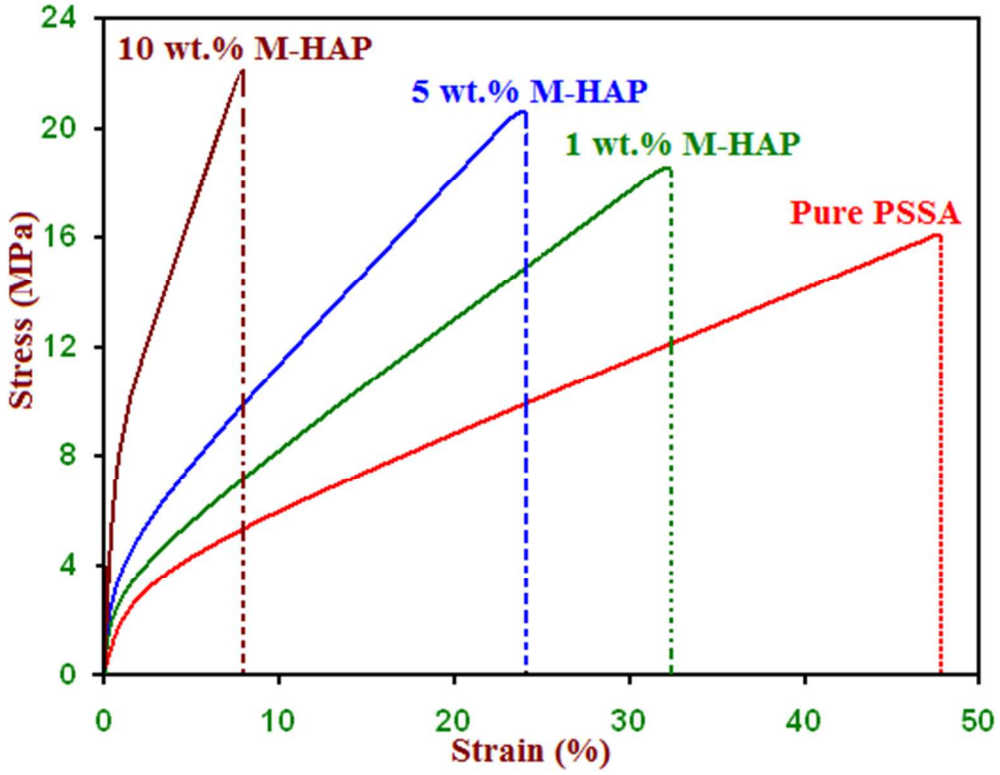

Fig.5 Mechanical strength of the M-HAP/PSSA nanocomposite

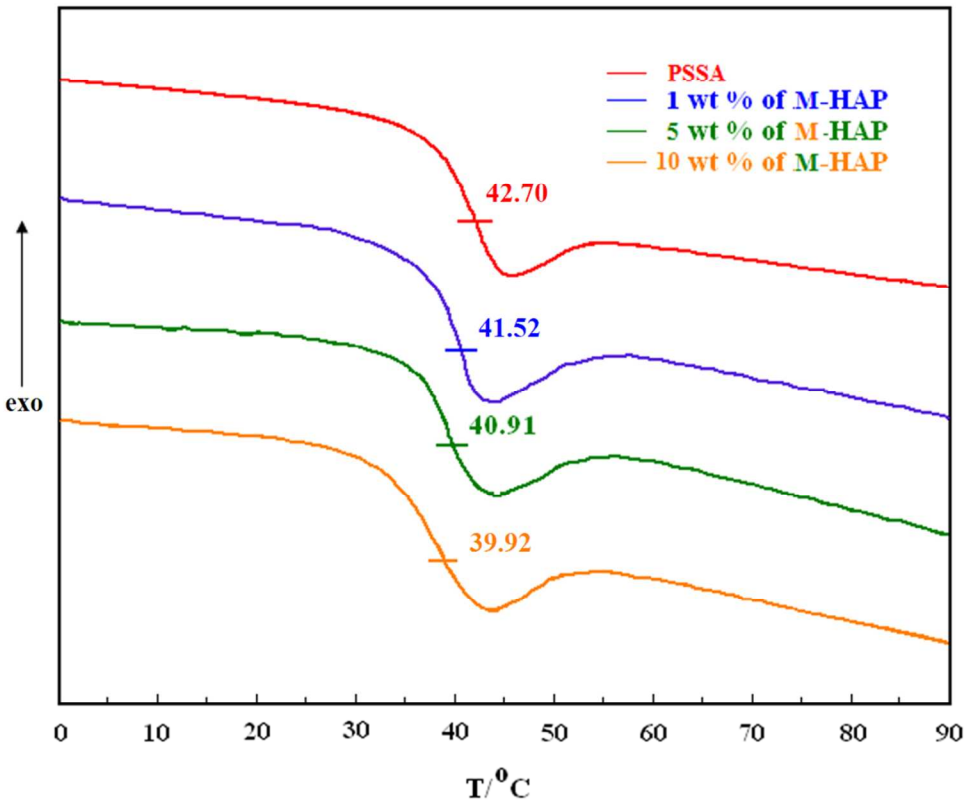

Fig.6 DSC curves of the M-HA/PSSA nanocomposite.

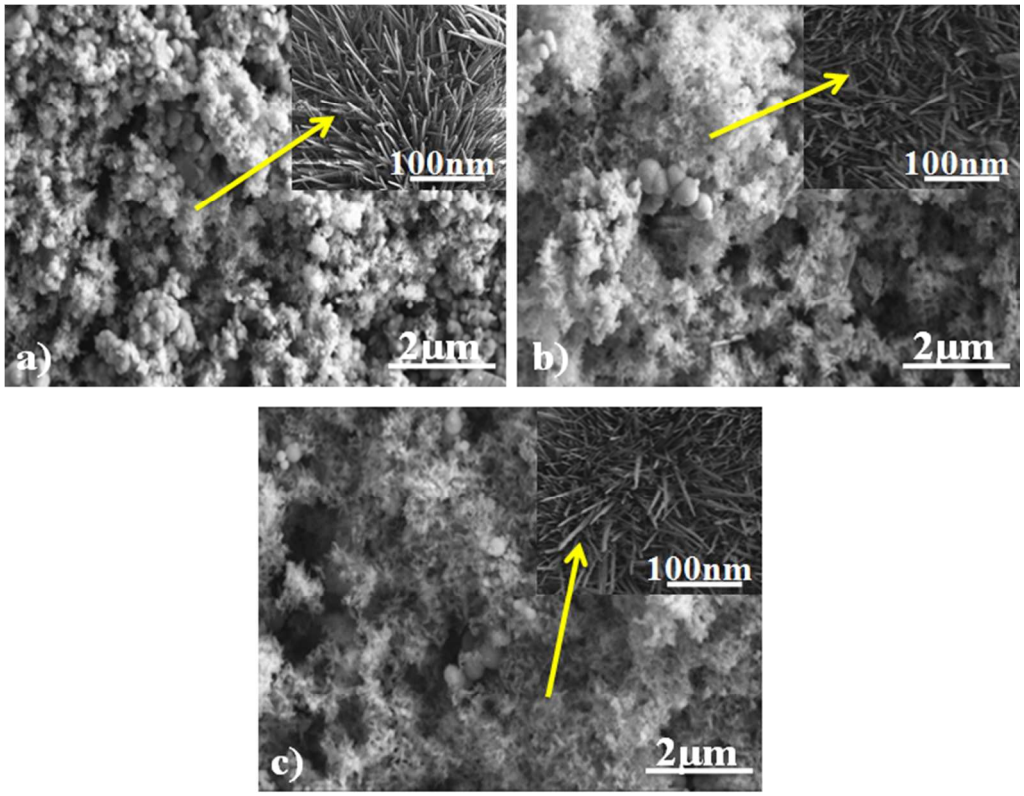

Fig.7 FESEM micrographs of 10 Wt% of M-HA in PSSA nanocomposite soaking in SBF solution (a) 1 day (b) 3 days and (c) 7 days (d) elemental composition nanocomposite 7 days soaking.

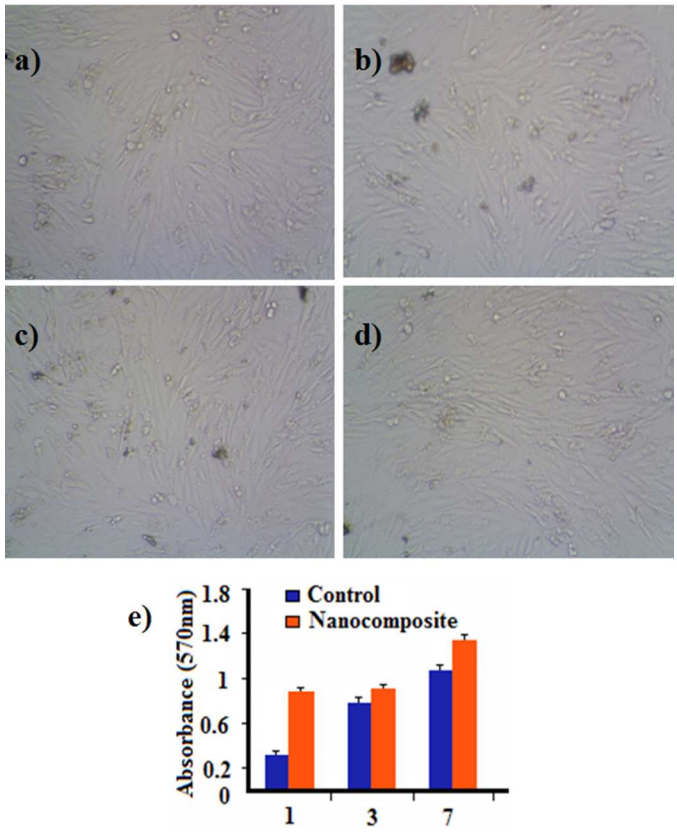

Fig.8 Optical images of MG63 on the M-HAP (10Wt. %)/ PSSA nanocomposite scaffold after in vitro culture for different days; (a) control (b) 1 day (c) 3 days and (d) 7 days (e) Bar diagram shows optical density of living cells. (control = without nanocomposites)